Journal of Applied Physics ARTICLE scitation.org/journal/jap

Schottky barrier height and modulation due to interface structure and defects in Pt|MgO|Pt heterojunctions with implications for resistive switching

Cite as: J. Appl. Phys. **127**, 205306 (2020); doi: 10.1063/1.5143658
Submitted: 26 December 2019 · Accepted: 7 May 2020 ·
Published Online: 27 May 2020

Manish K. Niranjan[a] and Ramesh Mamindla

AFFILIATIONS

Department of Physics, Indian Institute of Technology, Hyderabad 502285, India

[a]**Authors to whom correspondence should be addressed:** manish@iith.ac.in. **Tel.:** (91)040-23016092. **Fax:** (91)040-23016032

ABSTRACT

The modulation of Schottky barrier height (SBH) due to defect migration has been suggested to be an important driving mechanism for resistive switching in metal–oxide–metal structures. Here, we explore the SBH and its modulation due to different interface structures and defects in the Pt|MgO|Pt(001) system using hybrid Heyd–Scuseria–Ernzerhof density functional theory. The computed magnitudes of SBH at Pt|MgO interfaces obtained using the generalized gradient approximation (local density approximation) functional are found to be significantly underestimated as compared to those obtained using hybrid functional. Furthermore, the magnitudes of SBH are found to depend critically on interface structures. In the case of defect-free Pt|MgO interfaces, the *p*-type SBH is found to be 4.13 eV and 3.04 eV for interfaces having adjacent Pt–O and Pt–Mg bonds, respectively. In addition, the SBH magnitudes are found to exhibit significant variation primarily due to nominal effective charges on interface layers which, in turn, are induced by interface defects such as O and Mg vacancies. The magnitudes of *p*-type SBH are found to increase (decrease) by ∼1.0–1.5 eV as the ionic layers with charge +1e (−1e) are introduced at the interface. The modulation in SBH due to interface ionic/polar layer is explained using a micro-capacitor model. Furthermore, the SBH is found to shift by ∼0.2 eV with the varying distance of O and/or Mg vacancies from the interface. Our results suggest that fluctuations in experimental resistive switching data in Pt|MgO structures may originate due to fluctuations in SBH induced by changes in interface atomic structure. The study also shows that SBH in Pt|MgO and related structures may be modulated in a controlled way by the insertion of interface polar layers. The lower and upper bounds of the SBH magnitudes are also estimated using a semi-empirical model expressed in terms of parameters such as charge neutrality level, ionization potential, pinning parameter, and metal work function. The quantitative results on the SBH modulation presented in the study may be expected to have important implications for resistive switching phenomenon in Pt|MgO and similar other structures.

I. INTRODUCTION

In recent years, random access memory (ReRAM) devices based on resistance switching (RS) phenomena have generated much interest for applications as next generation nonvolatile memory devices.[1–4] In particular, nanoscale Pt|MgO|Pt metal–insulator–metal stack has emerged as a highly potential candidate for the development of next generation ReRAM devices.[2,3,5,6] In addition to the Pt|MgO|Pt structure, the resistive switching phenomenon has also been reported in other MgO based magnetic tunnel junctions.[7–9] Though resistive switching has been studied extensively due to its importance in abovementioned applications,[3,4,10] the fundamental understanding of this phenomenon is still far from being conclusive. Over the years, resistance switching behavior has been explained using various phenomenological models such as oxygen vacancy migration, charge trap/detrap, conducting domain, conductive filament percolation, and electrochemical migration of defects.[11–15] Recently, it has been suggested that resistive switching in metal–oxide–metal structures may originate due to changes in the Schottky barrier caused by the drift of

positively charged oxygen vacancies under the influence of the external electric field.[16,17] The Schottky barrier is reduced due to the creation of conducting channels as the vacancies drift toward the interface. However, the barrier is recovered due to annihilation of the channels as the vacancies drift away from the interface. In general, the Schottky barrier height (SBH) or band alignment across metal–oxide interface is an important interfacial parameter which critically influences the out-of-plane electrical transport and capacitance behavior due to exponential dependence of out-of-plane current on the SBH.[18] Over the last few decades, the formation of SBH has been extensively investigated in heterostructures, primarily based on Si, III–V, and II–VI semiconductors.[19–21] However, the microscopic physical mechanisms which drive the SBH formation at heterointerfaces are still not known conclusively.[19,20] In general, the control over the SBH modulation is highly desirable in order to manipulate transport properties in semiconductor and/or oxide based nanoelectronic devices.[18,20] Thus, the precise understanding of physical mechanisms of SBH formation is necessary in order to tune the SBH in these devices. In the last few decades, various empirical and phenomenological models have been proposed to explain SBH formation. However, it is now generally understood that the SBH formation and/or band offset is critically influenced by atomic and electronic structures of the metal–semiconductor (insulator) interface.[19,20] Therefore, the Schottky barrier modulation due to different interface structures, interfacial defects, and their migration can be expected to be the major driving mechanism for resistive switching in Pt|MgO|Pt structures due to large work function of Pt and a large bandgap of MgO.[10]

Here, in this article, we perform a comprehensive study of Schottky barrier formation and its modulation by different interface structures and interfacial defects in the Pt|MgO|Pt heterostructure within the framework of density functional theory (DFT). In particular, we first compute and analyze the SBH at two defect-free Pt|MgO interfaces using Heyd–Scuseria–Ernzerhof (HSE06) functional within the hybrid DFT framework. Thereafter, the modulation in SBH due to different interfacial defects such as oxygen vacancies, magnesium vacancies, substitutional defects, etc. is explored. Our results suggest that SBH at the Pt|MgO interface and thereby transport properties are quite sensitive to variation in the interface atomic structure. For instance, even in the absence of interface defects, the SBH is found to differ by ∼1.1 eV depending on whether the interface has Pt–O or Pt–Mg bonds. Furthermore, the SBH (*p*-type) is found to increase (decrease) as the vacancies such as oxygen (magnesium) are introduced at the interface. The modulations in SBH due to interface defects are explained using a semi-empirical micro-capacitor model.

The SBH modulation with varying interface structure is relevant for resistive switching phenomenon, since such a variation is expected due to creation and/or migration of defects resulting from external switching voltage. Though on the basis of experimental studies,[10] it is generally accepted that electronic barrier at the interface may play a critical role in resistive switching, no quantitative theoretical study has been reported on this subject to the best of our knowledge. Therefore, our study aims to provide accurate quantitative results which show the extent of variation in SBH and thereby electric resistance due to interface defects and interface structure in metal–oxide structures.

Over the years, band offset calculations at various S–S, I–I, M–S, and M–I (where M is the metal, S the semiconductor, and I the insulator) interfaces have been performed using the generalized gradient approximation (GGA) and/or local density approximation (LDA) within density functional theoretical (DFT) framework. However, the bandgaps estimated using GGA (LDA) functionals are significantly underestimated as compared to experimental values. The underestimation of bandgaps and resulting inaccuracy in band offsets is more severe for semiconductors and oxides with wide bandgaps such as MgO. Therefore, the Schottky barriers in Pt|MgO|Pt junctions computed using the GGA approximation are expected to be inaccurate by significant margin. Recently, it has been suggested that reasonably accurate estimates of band offsets in heterostructures can be obtained using hybrid functionals which mix a portion of nonlocal Hartree–Fock exchange with GGA exchange.[22–24] In addition to the hybrid functional DFT approach, we also employ a semi-empirical metal-induced-gap-states (MIGSs) model to estimate the SBH at the Pt|MgO interface. The MIGS model is expressed in terms of few parameters such as charge neutrality level in MgO, metal (Pt) work function, MgO ionization potential, and pinning parameter (S).

The rest of the paper is organized as follows. In Sec. II, the calculation methodology and details of interface models are presented. The *ab initio* calculations of SBH at defect-free Pt|MgO interfaces are presented in Sec. III A. The SBH modulation at Pt|MgO interfaces with oxygen, magnesium vacancies, and other polar defects are presented in Sec. III B. The estimates of SBH computed using the semi-empirical MIGS model are presented in Sec. IV. Finally, the concluding remarks are presented in Sec. V.

II. INTERFACE MODELS AND COMPUTATIONAL METHODOLOGY

The Pt|MgO interfaces are simulated by mirror symmetric supercells consisting 23 (or more) Pt layers on top of 31 (or more) MgO layers. A model of Pt|MgO heterostructure supercell and two possible interfaces are shown in Fig. 1. These two interfaces are indicated as type-A and type-B in the paper. In the case of type-A interface, Pt atoms are located adjacent (along the [001] direction) to Mg atoms and thus form Pt–Mg bonds. For type-B interface, Pt atoms are adjacent to O atoms and form Pt–O bonds. The interface vacancies as well as interface polar layers such as $(LaO)^{+1}$ are created by introducing appropriate defects on the interface MgO layer. The charge on these ionic layers is varied by using supercells with (2×1) and (2×2) surface/interface unit cells.

The density functional (DFT)[25] calculations are performed using plane wave basis set formalism and periodic boundary conditions as implemented in the VASP package.[26] The core–valence electron interactions are approximated using the projected augmented wave (PAW) method.[27] The exchange-correlation (xc) contributions are described using Heyd–Scuseria–Ernzerhof (HSE06) hybrid functional[28] and Perdew–Burke–Ernzerhof (PBE)[29] form of generalized gradient approximation. The plane wave basis set with a kinetic energy cutoff of 500 eV is used to expand Kohn–Sham orbitals. The Brillouin zones are sampled using a Monkhorst–Pack $(8/m) \times (8/n) \times 1$ *k*-meshe for total energy calculations of supercells with $(m \times n)$ interface unit cells. The calculations are

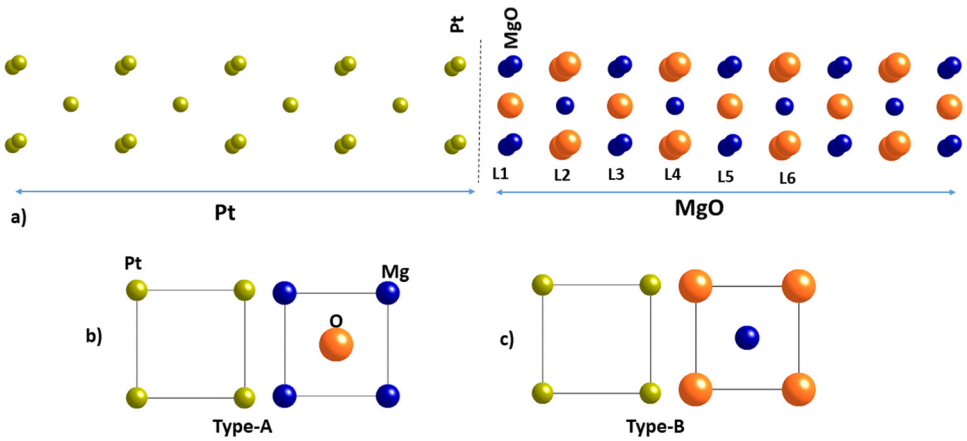

FIG. 1. (a) Side view of the atomic structure of the Pt|MgO(001) supercell with the (b) type-A interface and (c) type-B interface. Green, blue, and red balls indicate Pt, Mg, and O atoms, respectively.

converged to 10^{-6} eV/cell. The lattice parameters and atomic coordinates are relaxed until the largest force on each atom is reduced to less than 0.02 eV/Å. The planar averages of electrostatic potentials and layer density of states (LDOS) are used to estimate the Schottky barriers at the interfaces.[30–32]

III. RESULTS AND DISCUSSIONS

A. SBH at defect-free Pt|MgO interfaces

Next, we compute the SBH at Pt|MgO(001) interfaces. The interface atomic structure and Pt|MgO|Pt supercell are shown in Fig. 1. The p-type SBH ($\Phi_{B,p}$) and n-type SBH ($\Phi_{B,n}$) at metal–insulator interface may be computed using a macroscopic averaging (MA) approach as[24,33]

$$\Phi_{B,p} = \Delta E_p + \Delta V; \quad \Phi_{B,n} = E_g - \Phi_{B,p}, \tag{1}$$

where E_g is the bandgap of insulator (MgO) and ΔE_p is the bulk band structure term. In the case of metal–insulator (Pt–MgO) structure, ΔE_p may be obtained as the difference between Fermi energy of metal (Pt) and valence-band maximum of insulator (MgO) in bulk phase, measured from average electrostatic potential. ΔV is the electrostatic potential line-up term which is given as the difference between the average electrostatic potentials of MgO and Pt far from the interface in the Pt|MgO supercell. Usually, the bulk band structure term ΔE_p remains independent of interface structural details whereas the potential lineup ΔV may depend critically on structural details such as bonding between the atoms on interface layers. The potential line-up term (ΔV) has been suggested to be associated with the interfacial dipole which results from the charge transfer across the interface. As mentioned earlier, the accuracy in computed Φ_B or band lineups within the DFT framework crucially depends on the performance of the exchange-correlation (xc) functional. As is well known, the bandgaps of materials are severely underestimated when computed using GGA (LDA) xc-functionals. In the case of metal–semiconductor junctions with traditional semiconductors with small to medium bandgaps such as III–V compounds, silicon, etc., the errors in magnitudes of $\Phi_{B,p}$ computed using GGA (LDA) are relatively small.[34] However, if the semiconductor (insulator) has large bandgap, the errors in GGA (LDA) magnitudes of Φ_B can be significantly large.[35] The experimental bandgap of MgO is ~7.8 eV[36] and thus GGA (LDA) may not be reliable xc-functional to obtain Φ_B estimates at Pt|MgO heterointerfaces. The accurate bandgaps may be obtained using the screened hybrid functionals such as Heyd–Scuseria–Ernzerhof (HSE06).[28] However, in the case of superlattices with large number of atoms, the calculations usually become extremely expensive computationally and prohibitive at the hybrid functional level. Furthermore, optimum mixing parameter (α) in the hybrid functional calculation depends on the choice of the material, whereas superlattice simulating the interface consists more than single material. Thus, we compute Φ_B at the Pt|MgO interface using methodology recently suggested by Weston *et al.*[24] In this scheme, the band structure term ΔE_p is calculated using hybrid functional scheme, whereas ionic relaxations in the superlattice, and resulting potential lineup term ΔV is calculated using GGA functional. It was shown that the potential lineups computed using the GGA functional were in agreement within ~50 meV with those calculated using HSE hybrid functionals. Furthermore, even for heterostructures between materials with a large lattice mismatch, the potential lineups computed using GGA were found to be in close agreement with those computed using hybrid functionals.[24] Therefore, reasonably accurate magnitudes of band alignment or Φ_B at the Pt|MgO interface may be expected when computed by combining hybrid functional calculation of a bulk electronic band structure with potential lineup computed using GGA approximation. We first obtain the optimum mixing parameter (α_{opt}) for HSE06 functional by fitting the computed bandgap of MgO as a function of mixing parameter (α). The optimum value α_{opt} is found to be 0.43 for which computed MgO bandgap value (7.78 eV) comes out to be nearly equal to the experimental value (~7.8 eV).[36] As expected, the GGA bandgap of MgO ($\alpha = 0$ in HSE06 scheme) is found to be 4.74 eV which is underestimated by ~39% as compared to the experimental value. It may be noted that $\alpha = 0.25$ corresponds to standard setting in HSE06 scheme, for which the MgO bandgap is computed to be 6.47 eV. Table I shows the magnitudes of $\Phi_{B,p}$

TABLE I. Computed *p*-type SBH ($\Phi_{B,p}$) and *n*-type SBH ($\Phi_{B,p}$) in eV at type-A and type-B interfaces (see Fig. 1) in the MgO|Pt (001) supercell with and without defects.

Interface	Defect	$\Phi_{B,p}(\Phi_{B,n})$ Type-A	$\Phi_{B,p}(\Phi_{B,n})$ Type-B
$MgO\|(MgO)^{0}\|Pt$		3.05 (4.73)	4.14 (3.64)
$MgO\|(MgO_{1/2})^{+1.0}\|Pt$	$0.5 \times V\ddot{o}$	4.55 (3.23)	5.44 (2.34)
$MgO\|(Mg)^{+2.0}\|Pt$	$1.0 \times V\ddot{o}$	5.46 (2.32)	6.42 (1.36)
$MgO\|(Mg_{1/2}O)^{-1.0}\|Pt$	$0.5 \times V''_{Mg}$	2.88 (4.90)	3.51 (4.27)
$MgO\|(O)^{-2.0}\|Pt$	$1.0 \times V''_{Mg}$	2.77 (5.01)	3.12 (4.66)
$MgO\|(NaO)^{-1}\|Pt$	$1.0 \times Na'_{Mg}$	2.59 (5.19)	3.21 (4.57)
$MgO\|(KO)^{-1}\|Pt$	$1.0 \times K'_{Mg}$	2.68 (5.10)	3.26 (4.52)
$MgO\|(LaO)^{+1}\|Pt$	$1.0 \times La_{Mg}$	3.83 (3.97)	5.12 (2.66)
MgO|PtO–Mg|Pt		3.39 (4.39)	4.35 (3.43)

($\Phi_{B,n}$) for several Pt|MgO(001) interfaces computed using HSE06 hybrid functional scheme. As can be seen, the magnitudes of SBH for the type-A interface differ significantly (~1.1 eV) from that for the type-B interface. In our calculations, the type-B interface is found to be lower in energy by ~0.46 J/m^2 and hence relatively more stable than the type-A interface. This is expected due to stronger bonding between Pt and O atoms which are located adjacent to each other at the type-B interface as compared to bonding between Pt and Mg atoms at the type-A interface. The Pt–Mg (type-A) and Pt–O (type-B) bond lengths at the interface are found to be 2.92 Å and 2.44 Å, respectively. Furthermore, as discussed later, the charge transfer from Pt to O atoms is found to be higher as compared to that between Pt and Mg atoms. For defect-free interfaces, $\Phi_{B,p}$ ($\Phi_{B,n}$) are found to be 3.04 eV (4.74 eV) for type-A and 4.13 eV (3.65 eV) for type-B interfaces. The $\Phi_{B,p}$ for the type-B interface is higher by ~1.1 eV than that for the type-A interface. The higher magnitude of $\Phi_{B,p}$ for the type-B interface is expected due to the formation of stronger dipole which in turn results from higher charge transfer/redistribution between Pt–O bonds. Using the GGA approximation, the $\Phi_{B,p}$ for type-A and type-B interfaces are computed to be 0.84 eV and 1.93 eV, respectively. The computed values of $\Phi_{B,p}$ using the GGA approximation are significantly smaller (~2.5 eV) than those obtained using HSE06 hybrid xc-functional. The $\Phi_{B,p}$ may also be estimated from the layer projected density of states (LDOS) plot for Pt|MgO supercell.[30,37] In this approach, the $\Phi_{B,p}$ can be obtained as the difference between Fermi energy and valence-band edge in the MgO layer whose electronic structure approaches to that of bulk. Figure 2 shows the LDOS for the MgO layer farthest from the interface for type-A and type-B Pt|MgO supercells. As can be seen in Fig. 2, the GGA computed $\Phi_{B,p}$ values using the LDOS method are found to be 0.8 eV and 1.9 eV for type-A and type-B interfaces, respectively, and are in good agreement with values obtained using the macroscopic potential approach and the GGA approximation. As evident, the difference between the magnitudes of Φ_B for two interfaces is also found to be ~1.1 eV using the LDOS method. We have also computed $\Phi_{B,p}$ using higher energy cutoff up to 700 eV and higher k-mesh up to 16 × 16 × 1, in order to estimate the error due to numerical parameters. The variation in $\Phi_{B,p}$ is found to be less than ~5% as the energy cutoff and k-mesh are increased to higher values.

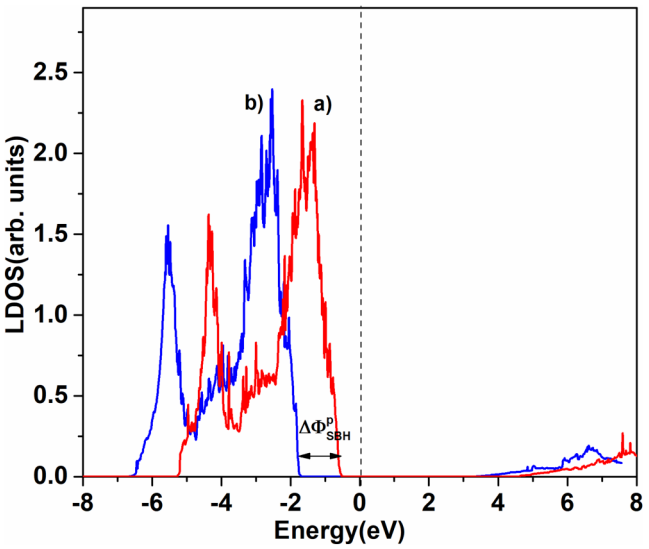

FIG. 2. Density of states (LDOS) projected on the MgO layer farthest from the interface in the Pt|MgO(001) supercell with (a) type-A and (b) type-B interfaces (see Fig. 1). The Fermi energy is indicated by the dotted line.

Next, in order to understand the large difference between SBHs (~1.1 eV) at two defect-free interfaces (type-A and type-B), we study the stepwise contribution of interfacial charge transfer and interfacial atomic relaxation to SBH using the approach as discussed in Refs. 38 and 39. The formation of the interface in the Pt|MgO supercell may be divided into three stages, i.e., "0," "1," and "2." In stage "0," MgO(001) and Pt(001) slabs with vacuum layers are considered separately and their atomic positions are relaxed. In stage "1," the separate MgO(001) and Pt(001) slabs with vacuum layers but having same atomic coordinates as that in relaxed Pt|MgO(001) supercell are considered. In this stage, the atomic relaxations transform the relaxed surface structure of stage "0" to the relaxed interface structure of the Pt|MgO supercell. Finally, the electronic relaxation takes place in stage "2," which results in charge transfer across the interface and thereby formation of the dipole. The $\Phi_{B,p}$ can be expressed with contribution from

each stage as

$$\Phi_{B,p} = \Phi_{B,p}^{(0)} + \Delta\Phi_{B,p}^{(1)} + \Delta\Phi_{B,p}^{(2)}. \quad (2)$$

The first term $\Phi_{B,p}^{(0)}$ is the $\Phi_{B,p}$ in stage "0." The $\Phi_{B,p}^{(0)}$ term is the Schottky–Mott limit of the SBH and can be calculated as the difference between the ionization potential (I_S) of MgO(001) and work function (ϕ_M) of Pt(001) surfaces,

$$\Phi_{B,p}^{(0)} = I_S - \phi_M. \quad (3)$$

The correction to the ideal Schottky–Mott limit of SBH ($\Phi_{B,p}^{(0)}$) due to atomic relaxations is indicated by $\Delta\Phi_{B,p}^{(1)}$ in stage "1," whereas $\Delta\Phi_{B,p}^{(2)}$ indicates the correction to ($\Phi_{B,p}^{(0)}$) due to electronic relaxations in stage "2." The $\Delta\Phi_{B,p}^{(1)}$ and $\Delta\Phi_{B,p}^{(2)}$ can be expressed as

$$\Delta\Phi_{B,p}^{(1)} = \Delta I_S^{(1)} - \Delta\phi_M^{(1)}; \quad \Delta\Phi_{B,p}^{(2)} = \Delta V^{(2)} - \Delta\phi_M^{(2)}, \quad (4)$$

where $\Delta I_S^{(1)}$and $\Delta\phi_M^{(1)}$ are the change in MgO(001) ionization potential and Pt(001) work function, respectively, as the surface atomic structures are transformed from their equilibrium configuration (stage "0") to interface-like configurations (stage "1"). Similarly, $\Delta V^{(2)}$ is the shift in the electrostatic potential across the interface due to redistribution of electron density in stage "2" (electronic relaxations). Likewise, the $\Delta\phi_M^{(2)}$ is the possible change in Pt (metal) work function due to shift in the Fermi level. Table II shows the computed values of abovementioned quantities associated with contribution of atomic and electronic relaxations to Φ_B^p. The computed value of $\Phi_{B,p}^{(0)}$ (the Schottky–Mott limit) is found to be 1.93 eV. In the Schottky–Mott limit, the transfer of charge across the interface is not considered. The magnitude of $\Phi_{B,p}^{(0)}$ indicates that atomic and electronic relaxations at the interface may contribute significantly to Φ_B^p for both interfaces. As can be seen, the ionization potential of MgO(001) is shifted by −0.39 eV (−1.61 eV) for the type-A (type-B) interface in stage "1," as the relaxed equilibrium MgO structure is changed to that in the relaxed Pt|MgO supercell. The decrease in the ionization potential for the type-B interface is ∼1.2 eV as compared to that for the type-A interface. In stage "1," the work function of the Pt(001) surface is shifted by +0.17 eV for type-A and +0.09 eV for type-B interfaces due to atomic relaxations. Thus, the *p*-type SBH is reduced from the Schottky–Mott limit ($\Phi_{B,p}^{(0)}$) by 0.56 eV (1.7 eV) for the type-A (type-B) interface in stage "1" due to atomic relaxations. However, the large interface dipole is induced by the electronic relaxations which increases the *p*-type SBH ($\Delta\Phi_{B,p}^{(2)}$) by 1.68 eV (3.92 eV) for the type-A (type-B) interface. It is interesting to note that *p*-type SBH is reduced by ∼1.1 eV due to atomic rearrangement but increased by ∼2.2 eV due to electronic rearrangement in the case of the type-B interface as compared to that for the type-A interface. Figure 3 shows the planar average electron density difference and interface dipole due to electronic charge transfer in the Pt|MgO(001) system with type-A and type-B interfaces. As evident from Fig. 3, the charge transfer is much higher for the type-B interface as compared to that for the type-A interface. The higher charge transfer for the type-B interface with interfacial Pt–O bonds as compared to that for the type-A interface with Pt–Mg bonds is expected due to relatively larger electronegativity of O atoms than Mg atoms. Furthermore, the charge transfer is confined to ∼1–2 MgO planes to ∼3–4 Pt planes from the interface. Figure 3 also shows the modulation in induced charge density in Pt side of the Pt|MgO system. The modulation in induced charge density may be indicative of Friedel oscillations.

TABLE II. Contributions from ionic and electronic relaxations to the *p*-SBH at the Pt|MgO interface (see Sec. III and Eqs. (2)–(4)].

	Stage 0	Stage 1			Stage 2		
	$\Phi_{B,p}^{(0)}$	$\Delta I_S^{(1)}$	$\Delta\phi_M^{(1)}$	$\Delta\Phi_{B,p}^{(1)}$	$\Delta V^{(2)}$	$\Delta\phi_M^{(2)}$	$\Delta\Phi_{B,p}^{(2)}$
Interface-A	+1.92	−0.39	+0.17	−0.56	+1.68	0.00	+1.68
Interface-B	+1.92	−1.61	+0.09	−1.70	+3.92	0.00	+3.92

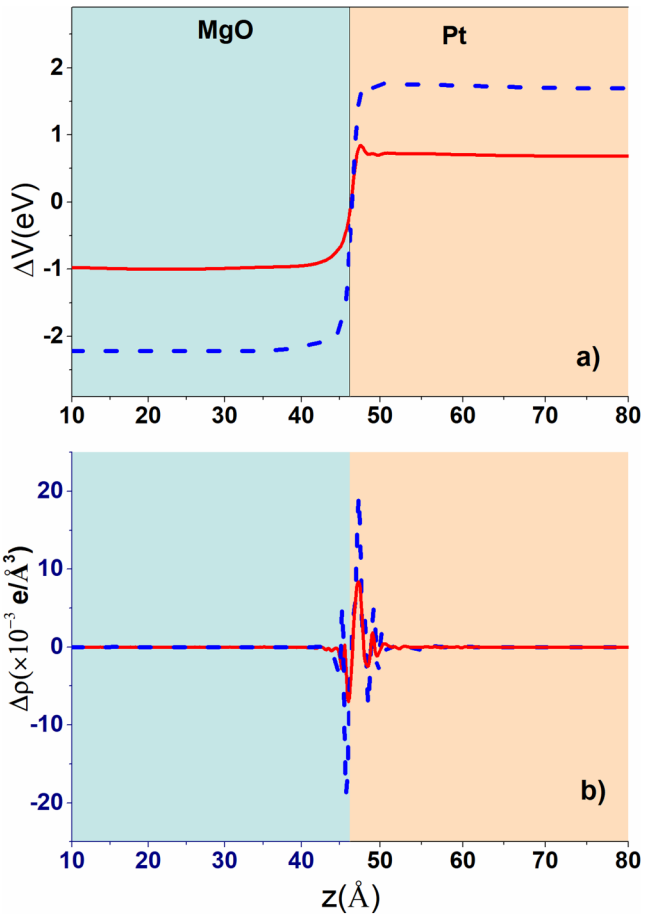

FIG. 3. Change in the (a) electrostatic potential (planar averaged) and (b) charge densities (planar averaged) in the MgO|Pt supercell during stage "2" due to redistribution of the electronic density [see Sec. III and Eqs. (2)–(4)]. The dotted vertical line indicates the MgO|Pt interface.

Presently, these computed values may not be compared with experimental values as no experimental study on $\Phi_{B,p}$ ($\Phi_{B,n}$) in the Pt|MgO(001) system has been reported to the best of our knowledge. However, in order to assess the accuracy of this method, we have also calculated $\Phi_{B,p}$ ($\Phi_{B,n}$) for the Ag|MgO(001) interface for which experimental magnitude of $\Phi_{B,p}$ has been reported recently.[40] Using similar numerical parameters such as supercell size, energy cutoff, k-mesh, etc. as those used for the Pt|MgO(001) supercell, the computed value of $\Phi_{B,p}$ in the Ag|MgO(001) supercell comes out to be 3.78 eV and 4.74 eV for type-A and type-B interfaces, respectively. Incidentally, the computed value of $\Phi_{B,p}$ for the type-A interface is in close agreement with the reported experimental value of 3.85 $\pm$ 0.1 eV. Thus, it may be expected that the computed magnitudes of $\Phi_{B,p}$ ($\Phi_{B,n}$) at Pt|MgO(001) interfaces will also exhibit similar comparative trend with the experimental data. However, it may be noted that the direct comparison of theoretical estimates of SBH with corresponding experimental results may be tricky and ambiguous, if the experimental interface atomic structure is not specified. This is primarily due to critical influence of interface atomic structures on the SBH magnitudes as further discussed in Sec. III B.

B. SBH modulation due to interface defects and polar layers

Next, we study the modulation in the SBH at the Pt|MgO interface due to various interfacial defects such as oxygen vacancies ($V\ddot{o}$), magnesium vacancies (V'_{Mg}), and other substitutional polar defects. As discussed earlier, the SBH modulation due to these defects may have important implications for resistive switching in Pt|MgO structures due to migration of defects (such as oxygen vacancies) under the influence of external electric field.[10] Table I and Fig. 4 show the computed $\Phi_{B,p}$ ($\Phi_{B,n}$) for different interface structures, interface O (Mg) vacancies, and other substitutional defects. It may be noted that the magnitudes of computed $\Phi_{B,p}$ ($\Phi_{B,n}$) for various interface defects shown in Table I and Fig. 4 indicate only the qualitative trend. These values may not be quantitatively accurate due to errors which may result from electrostatic interactions of defects, wave function overlap, etc.[41] The errors may be expected due to relatively small size of interface supercells which are used to simulate the interface defects in our calculations. As can be seen, the vacancies and other defects in the MgO plane transform it from being neutral to ionic. For instance, neutral MgO plane turns into polar $(MgO_{1/2})^{+1.0}$ plane with +1e charge due to vacancy of one O atom per (2 × 1) neutral MgO plane. As evident from Table I, the magnitude of $\Phi_{B,p}$ increases (decreases) for the interface ionic layer with positive (negative) charge. For the MgO|$(MgO_{1/2})^{+1.0}$|Pt supercell, the $\Phi_{B,p}$ ($\Phi_{B,n}$) is computed to be 4.55 eV (3.23 eV) and 5.44 eV (2.34 eV) for type-A and type-B interfaces, respectively. For the type-A interface, the $\Phi_{B,p}$ ($\Phi_{B,n}$) is higher (lower) by ∼1.3–1.5 eV as compared to that for the non-polar Pt|MgO interface. Similarly, for the type-B interface, the magnitude of $\Phi_{B,p}$ ($\Phi_{B,n}$) is higher (lower) by ∼1.0–1.8 eV. On the other hand, in the case of MgO|$(Mg_{1/2}O)^{-1.0}$|Pt supercell, the $\Phi_{B,p}$ ($\Phi_{B,n}$) is computed to be 2.88 eV (4.90 eV) and 3.51 eV (4.27 eV) for type-A and type-B interfaces, respectively. Thus, the magnitude of $\Phi_{B,p}$ ($\Phi_{B,n}$) is reduced (increased) by 0.16–0.64 eV for the interface polar layer with charge −1e. Likewise, in the case of MgO|$(NaO)^{-1.0}$|Pt and MgO|$(KO)^{-1.0}$|Pt supercells, $\Phi_{B,p}$ ($\Phi_{B,n}$) is decreased (increased) by ∼0.4–0.9 eV. In these supercells, the $(NaO)^{-1}$ and $(KO)^{-1}$ layers are created by replacing Mg atoms on the $(MgO)^0$ layer with Na or K atoms. The computed positive or negative shifts in Φ_B due to interfacial ionic layers are in qualitative agreement with recent experimental results on Φ_B in the $SrTiO_3$|$SrRuO_3$ structure.[42] The obtained results also suggest that SBH can be modulated in a controlled way by the insertion of interface polar layers.

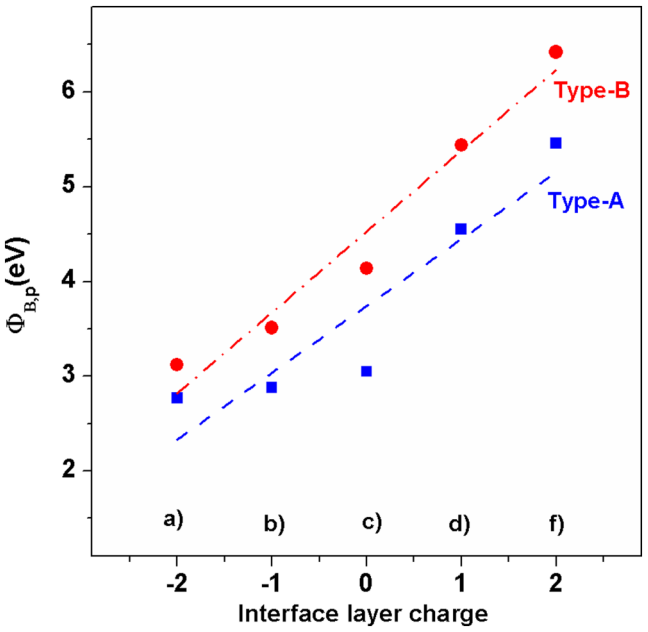

FIG. 4. The *p*-type SBH ($\Phi_{B,p}$) at type-A and type-B interfaces in the MgO|(IPL)|Pt (001) supercell with the interface polar layer (IPL). The number on the *x* axis indicates the charge on the interface polar layer.

We have also computed the change in SBH, i.e., $\Delta\Phi_B$ due to single O vacancy ($V\ddot{o}$) per (2 × 1) interface cell as a function of distance of O vacancy from the interface. The computed results are shown in Fig. 5. As discussed earlier, Fig. 5 is only indicative of qualitative trend of variation in $\Delta\Phi_B$ as the vacancies move away from the interface. For V_O at the first layer (L1) from the interface, $\Delta\Phi_{B,p}$ is 1.31 eV, whereas for V_O at the sixth layer (L6) from interface, $\Delta\Phi_{B,p}$ is 1.81 eV. The magnitude of $\Delta\Phi_{B,p}$ is decreased by 0.28 eV as V_O changes from the first layer (L1) to the second layer (L2) and increased by 0.20 eV with V_O shifting from the second layer (L2) to the third layer (L3). It may be noted that qualitatively similar modulation in Φ_B with O vacancy and its distance from the interface has also been reported for some oxide structures such as $SrRuO_3$|$SrTiO_3$.[43] The observed modulation in $\Delta\Phi_{B,p}$ and thereby resistance due to variation of V_O distance from the interface may have relevance for fluctuations in resistive switching generally observed in experiments.[10] Figure 5 also shows the $\Delta\Phi_{B,p}$ due to single Mg vacancy (V''_{Mg}) per (2 × 1) interface cell as a function of increasing distance from the interface. As can be seen, the

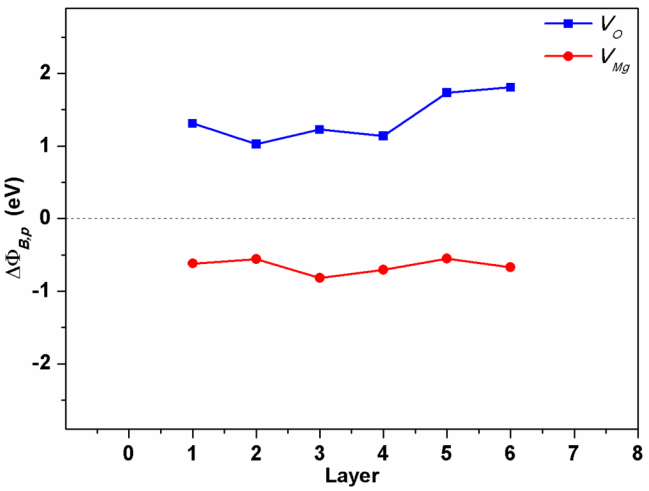

FIG. 5. The shift in the *p*-type SBH (blue squares) in the $(MgO)_{31}|(Pt)_{23}-(2\times1)$ supercell as a single $(MgO)^0$ plane is replaced by the $(MgO_{1/2})^{+1.0}$ plane. The shift in the *p*-type SBH (red circles) in the $(MgO)_{31}|(Pt)_{23}$ supercell as a single $(MgO)^0$ plane is replaced by the $(Mg_{1/2}O)^{-1.0}$ plane. The number on the *x* axis indicates the $(MgO_{1/2})^{+1.0}$ or $(Mg_{1/2}O)^{-1.0}$ plane from the interface.

magnitude of $|\Delta\Phi_{B,p}|$ is much smaller in the case of V_{Mg} than that for V_o. The $\Delta\Phi_{B,p}$ is −0.62 eV and −0.67 eV for V_{Mg} at the first layer (L1) and the sixth layer (L6), respectively, from the interface. The $\Delta\Phi_{B,p}$ increases by 0.06 eV as V_{Mg} changes from the first layer (L1) to the second layer (L2) and decreases by 0.26 eV as V_{Mg} changes from the second layer (L2) to the third layer (L3). The computed modulations in $\Phi_{B,p}$ at the Pt|MgO interface due O or Mg vacancies are expected and may be understood using a microscopic capacitor model.[44,45] The single O atom vacancy on neutral $(MgO)^0-(2\times1)$ plane transforms it to $(MgO_{1/2})^{+1}-(1\times1)$, which is a polar interface plane with charge +1e. The interface polar layer produces a bare ionic dipole, ΔV_b, which shifts $\Phi_{B,p}$ by $\Delta\Phi_B$,

$$\Delta\Phi_B \cong \frac{\Delta V_b}{\varepsilon_{eff}} = \frac{qe(a/2)}{\varepsilon_{eff}\varepsilon_0(a^2)}, \tag{5}$$

where a, ε_0, ε_{eff}, and q are lattice constant, vacuum permittivity, effective dielectric (screening) constant, and dipole charge (or charge on interface plane), respectively. The ε_{eff} in the region around the Pt|MgO interface may be estimated as

$$\varepsilon_{eff}(z) = \varepsilon_\infty^{(MgO)} + \frac{e^2 D_S(z)\delta}{\varepsilon_0}, \tag{6}$$

where $\varepsilon_\infty^{(MgO)}$ is the electronic dielectric constant of MgO, $D_S(z)$ is the density of surface states estimated at the position (z) of the dipole, and δ is the decay length. The approximate values of $D_S(z)$ and δ may be estimated from the interface electronic structure for the Pt|MgO(001) system. Figure 6(a) show the density of states (LDOS) projected on the interface MgO layer and on the MgO layer farthest from interface in the Pt|MgO(001) supercell. The electronic structure of the MgO layer farthest from the interface approaches to that of bulk MgO. Figure 6(b) shows the band structure for the Pt|MgO(001) supercell with projected bulk MgO states. The states seen in the bandgap of MgO can be identified as metal-induced-gap-states (MIGSs) in Fig. 6(b).[19,20] Figure 6(c) shows the planar averaged charge density contributed by some of these MIGS states at the Fermi energy (~0 eV). The MIGS density and decay length are found to be $\sim0.2\times10^{14}\,cm^{-2}$ and ~3 Å, respectively. The computed magnitude of the MIGS density is small which indicates that the Fermi-level pinning in the Pt|MgO system is significantly weak. This result is consistent with the large modulation in computed Φ_B with change in the interface structure as discussed earlier.[19,20] The approximate values of $D_S(z)$ and δ are found to be $\sim0.04\,Å^{-2}\,eV^{-1}$ and ~3.0 Å which are estimated from the layer density of states and the charge density (planar averaged) corresponding to MIGS states [see Figs. 6(a)–6(c)]. Using $\varepsilon_\infty^{(MgO)} \sim 3.2$,[46] the effective dielectric constant is estimated to be ~26. Thus, the magnitude of $\Phi_{B,p}$ ($\Phi_{B,n}$) is increased (decreased) by ~1.1 eV due to the polar $(MgO_{1/2})^{+1}$ layer formed by oxygen vacancy V_O on the neutral $(MgO)^0$ layer. The shift in $\Phi_{B,p}$ ($\Phi_{B,n}$) estimated from the microscopic capacitor model is in qualitative agreement with that computed from first principles calculations. However, it may be noted that the accurate estimation of $D_S(z)$ and δ and thereby $\Delta\Phi_b$ from the DOS and projected charge density plots may be somewhat ambiguous. Thus, the estimate of $\Delta\Phi_b$ obtained from the microscopic capacitor model may not be directly compared with corresponding *ab initio* and/or experimental values. Nevertheless, the micro-capacitor model can be used to qualitatively explain the shift in $\Phi_{B,p}$ ($\Phi_{B,n}$) due to charge on the interface polar layer.

IV. EMPIRICAL MODEL ESTIMATE OF SBH

Over the years, few empirical models have been used to obtain estimates of $\Phi_{B,p}$ at metal–semiconductor heterointerfaces. For instance, it has been suggested that $\Phi_{B,p}$ may be expressed in terms of parameters such as charge neutrality level (φ_{CNL}), pinning parameter (S), metal work function (φ_M), and ionization potential (I) of the insulator as[18–20]

$$\Phi_{B,p} = \varphi_{CNL} - S(\varphi_M - I + \varphi_{CNL}). \tag{7}$$

The pinning parameter (S) is characteristic of the insulator (MgO). The magnitude of S describes the screening by interfacial states and is bounded by values 0 and 1. An estimate of S may be obtained from the empirical relation proposed by Monch,[47]

$$S = \frac{1}{1+0.1(\varepsilon_\infty+1)^2}, \tag{8}$$

where ε_∞ is the electronic dielectric constant of insulator (MgO). The value $S=1$ is the Schottky–Mott limit of SBH and indicates no transfer of charge across the interface. On the other hand, $S=0$ indicates the complete pinning of the Fermi level at the charge neutrality level (φ_{CNL}). The strong pinning limit $S=0$ in Eq. (7) results in $\Phi_{B,p}=\varphi_{CNL}$. The magnitude of S is computed to be 0.35 using $\varepsilon_\infty=3.2$ for MgO.[46] The computed values of φ_M for Pt

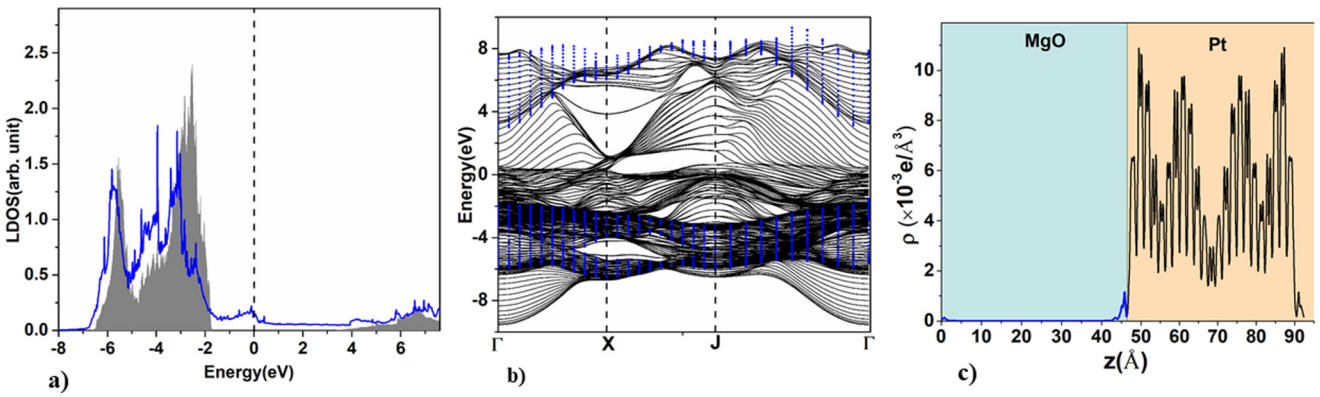

FIG. 6. (a) Density of states (LDOS) projected on the interface MgO layer (blue line) and MgO layer farthest from the interface (the shaded area) in the Pt|MgO(001) supercell with the type-B interface. The Fermi energy is indicated by the dotted line. (b) The band structure for the Pt|MgO(001) system. The blue dots indicate the projected bulk MgO states. (c) Charge density (planar averaged) corresponding to Pt|MgO bonds (MIGS states) shown in (b) near ∼0 eV (the Fermi energy).

(001) and I for MgO(001) are found to be 5.74 eV and 7.59 eV, respectively. The computed values differ by 2.7% and 6.1% with reported experimental values $\varphi_M = 5.9$ eV for Pt[48] and $I = 7.15$ eV for MgO, respectively.[40] By identifying φ_{CNL} with the branch-point energy in the quasi-particle band structure, its magnitude has been reported to be 5.4 eV.[49] However, the φ_{CNL} has also been suggested to be at the bandgap center in some reports which gives its value as 3.15 eV.[50] Using $\varphi_{CNL} = 5.4$ eV and computed (experimental) values of φ_M and I, the magnitude of $\Phi_{B,p}$ at the Pt|MgO(001) interface comes out to be 4.12 eV (3.91 eV). This value of $\Phi_{B,p}$ computed using the semi-empirical model is found to be in close agreement with that obtained from first principles for the type-B interface. On the other hand, using $\varphi_{CNL} = 3.15$ eV, the $\Phi_{B,p}$ comes out to be 3.15 eV (2.93 eV), which is in close agreement with that obtained from first principles for the type-A interface.

V. CONCLUSIONS

Using hybrid density functional theory, the Schottky barrier height (SBH) and its modulation due to interface structures and interface defects are explored in the Pt|MgO(001) heterostructure. The magnitudes of SBH computed using GGA functional are found to be significantly underestimated as compared to those obtained using the hybrid functional scheme. The SBH magnitudes are computed for two types of defect-free Pt|MgO interfaces: type-A with adjacent Pt and Mg atoms (along [001] direction) and type-B with adjacent Pt and O atoms at the interface. The SBH is found to be critically influenced by the interface structure. For defect-free interfaces, the p-type SBH is found to be 4.13 eV for the type-B interface and 3.05 eV for the type-A interface. In the case of interface defects, significant modulation in SBH is found primarily due to charge on the interface layer, which in turn depends on the interface defects such as O and Mg vacancies. The p-type SBH is found to increase (decrease) by ∼1.0–1.5 eV as the neutral interface MgO layer is transformed to the polar layer with +1e (−1e) charge due to defects. A micro-capacitor model is used to qualitatively explain the modulation in SBH due to the charged interface layer. A modulation of ∼0.2 eV in the SBH is computed as the distance of O and/or Mg vacancies from the interface is increased. The results suggest that SBH can be modulated in a controlled way by the insertion of interface polar layers. The SBH for the Pt|MgO system is also estimated using a semi-empirical model that is expressed in terms of parameters such as charge neutrality level, ionization potential, pinning parameter, and metal work function. The presented results on the SBH modulation due to various factors may have important implications for resistive switching in Pt|MgO and other metal–oxide structures. We hope that the present work will stimulate further theoretical and experimental studies on SBH modulation and its influence on resistive switching in metal–oxide and other similar structures.

ACKNOWLEDGMENTS

This work was supported by the UGC-DAE Consortium for Scientific Research and Department of Science and Technology (DST), Government of India.

DATA AVAILABILITY

The data that support the findings of this study are available within the article.

REFERENCES

[1]W. W. Zhuang *et al.*, in *Technical Digest—International Electron Devices Meeting* (IEEE, 2002), p. 193.
[2]H. Akinaga and H. Shima, "Resistive random access memory (ReRAM) based on metal oxides," Proc. IEEE **98**, 2237 (2010).
[3]A. Sawa, "Resistive switching in transition metal oxides," Mater. Today **11**, 28 (2008).
[4]R. Waser *et al.*, "Redox based resistive switching memories-nanoionic mechanisms, prospects, and challenges," Adv. Mater. **21**, 2632 (2009).
[5]H.-H. Huang *et al.*, "Nonpolar resistive switching in the Pt/MgO/Pt nonvolatile memory device," Appl. Phys. Lett. **96**, 193505 (2010).
[6]F.-C. Chiu *et al.*, "Conduction mechanism of resistive switching films in MgO memory devices," J. Appl. Phys. **111**, 094104 (2012).

[7]P. Krzysteczko *et al.*, "Memristive switching of MgO based magnetic tunnel junctions," Appl. Phys. Lett. **95**, 112508 (2009).
[8]C. Yoshida *et al.*, "Unipolar resistive switching in CoFeB/MgO/CoFeB magnetic tunnel junction," Appl. Phys. Lett. **92**, 113508 (2008).
[9]J. M. Teixeira *et al.*, "Electroforming, magnetic and resistive switching in MgO-based tunnel junctions," J. Phys. D **42**, 105407 (2009).
[10]J. S. Lee *et al.*, "Resistive switching phenomena: A review of statistical physics approaches," Appl. Phys. Rev. **2**, 031303 (2015).
[11]M. J. Rozengerg *et al.*, "Nonvolatile memory with multilevel switching: A basic model," Phys. Rev. Lett. **92**, 178302 (2004).
[12]M. J. Lee *et al.*, "Electrical manipulation of nanofilaments in transition-metal oxides for resistance-based memory," Nano Lett. **9**, 1476 (2009).
[13]N. Xu *et al.*, "Characteristics and mechanism of conduction/set process in TiN/ZnO/PtTiN/ZnO/Pt resistance switching random-access memories," Appl. Phys. Lett. **92**, 232112 (2008).
[14]K. Szot *et al.*, "Switching the electrical resistance of individual dislocations in single- crystalline $SrTiO_3$," Nat. Mater. **5**, 312 (2006).
[15]T. Fujii *et al.*, "Hysteretic current-voltage characteristics and resistance switching at an epitaxial oxide Schottky junction $SrRuO_3/SrTi_{0.99}Nb_{0.01}O_3$," Appl. Phys. Lett. **86**, 012107 (2005).
[16]J. J. Yang *et al.*, "Memristive switching mechanism for metal/oxide/metal nanodevices," Nat. Nanotechnol. **3**, 429 (2008).
[17]J. J. Yang *et al.*, "A family of electronically reconfigurable nanodevices," Adv. Mater. **21**, 3754 (2009).
[18]S. M. Sze, *Physics of Semiconductor Devices*, 2nd ed. (Wiley, New York, 1981).
[19]R. T. Tung, "The physics and chemistry of Schottky barrier height," Appl. Phys. Rev. **1**, 011304 (2014).
[20]R. T. Tung, "Recent advances in Schottky barrier concepts," Mater. Sci. Eng. **35**, 1 (2001).
[21]M. K. Niranjan *et al.*, "Theoretical investigation of PtSi surface energies and work functions," Phys. Rev. B **73**, 195332 (2006).
[22]A. Alkauskas, P. Broqvist, F. Devynck, and A. Pasquarello, Phys. Rev. Lett. **101**, 106802 (2008).
[23]P. G. Moses, M. Miao, Q. Yan, and C. G. Van de Walle, J. Chem. Phys. **134**, 084703 (2011).
[24]L. Weston *et al.*, "Accurate and efficient band-offset calculations from density functional theory," Comput. Mater. Sci. **151**, 174–180 (2018).
[25]W. Kohn and L. J. Sham, "Self consistent equations including exchange and correlation effects," Phys. Rev. **140**, A1133 (1965).
[26]G. Kresse and J. Furthmuller, "Efficient iterative schemes for *ab initio* total energy calculations using a plane-wave basis set," Phys. Rev. B **54**, 11169 (1996).
[27]P. E. Blöchl, "Projector augmented-wave method," Phys. Rev. B **50**, 17953 (1994).
[28]J. Heyd, G. E. Scuseria, and M. Ernzerhof, J. Chem. Phys. **124**, 219906 (2006).
[29]J. P. Perdew *et al.*, Phys. Rev. Lett. **77**, 3865 (1996).
[30]M. Peresso *et al.*, "Band engineering at interfaces: Theory and numerical experiments," J. Phys. D Appl. Phys. **31**, 1273–1299 (1998).
[31]V. S. Kumar and M. K. Niranjan, "Effect of surface structure on workfunction and Schottky-barrier height in $SrRuO_3/SrTiO_3$ (001) heterojunctions," J. Appl. Phys. **115**, 173705 (2014).
[32]M. K. Niranjan, "Interface electronic structure and Schottky-barrier height in Si/NiSi(010) and Si/PtSi(010) heterostructures: A first-principles theoretical study," Superlattices Microstruct. **100**, 808–817 (2016).
[33]M. K. Niranjan *et al.*, "Ab initio study of atomic structure and Schottky barrier height at the $GaAs/Ni_{0.5}Pt_{0.5}Ge$ interface," Phys. Rev. B **77**, 155316 (2008).
[34]C. G. Van de Walle and R. M. Martin, Phys. Rev. B **35**, 8154 (1987).
[35]Y. Hinuma, A. Grüneis, G. Kresse, and F. Oba, Phys. Rev. B **90**, 155405 (2014).
[36]R. C. Whited, C. J. Flaten, and W. C. Walker, Solid State Commun. **13**, 1903 (1973).
[37]M. K. Niranjan *et al.*, "Relation between the work function and Young's modulus of RhSi and estimate of Schottky-barrier height at RhSi/Si interface: An *ab-initio* study," J. Appl. Phys. **112**, 093702 (2012).
[38]M. Mrovec *et al.*, "Schottky barriers at transition-metal/$SrTiO_3$ (001) interfaces," Phys. Rev. B **79**, 245121 (2009).
[39]V. S. Kumar and M. K. Niranjan, "Precise control of Schottky barrier height in $SrTiO_3/SrRuO_3$ heterojunctions using ultrathin interface polar layers," J. Phys. D Appl. Phys. **49**, 255302 (2016).
[40]T. Jaouen *et al.*, "Work function shifts, Schottky barrier height, and ionization potential determination of thin MgO films on Ag(001)," Appl. Phys. Lett. **97**, 232104 (2010).
[41]C. Freysoldt *et al.*, "First-principles calculations for point defects in solids," Rev. Mod. Phys. **86**, 253 (2014).
[42]T. Yajima T *et al.*, "Controlling band alignments by artificial interface dipoles at perovskite heterointerfaces," Nature Commun. **6**, 6759 (2015).
[43]S. H. Jeon *et al.*, "First-principles modeling of resistance switching in perovskite oxide material," Appl. Phys. Lett. **89**, 042904 (2006).
[44]A. M. Cowley and S. M. Sze, "Surface states and barrier height of metal semiconductor systems," J. Appl. Phys. **36**, 3212 (1965).
[45]C. Berthod *et al.*, "Schottky barrier heights at polar metal/semiconductor interfaces," Phys. Rev. B **68**, 085323 (2003).
[46]O. L. Anderson and P. Glynn, J. Phys. Chem. Solids **26**, 1961 (1965).
[47]W. Mönch, "Role of virtual gap states and defects in metal-semiconductor contacts," Phys. Rev. Lett. **58**, 1260 (1987).
[48]"Work functions measurement and results," in *Solid State Surface Science*, edited by J. C. Riviere and M. Green (Decker, New York, 1969), Vol. 1.
[49]A. Schleife *et al.*, Appl. Phys. Lett. **94**, 012104 (2009).
[50]J. Tersoff, "Schottky barrier heights and the continuum of gap states," Phys. Rev. Lett. **52**, 465 (1984).